Geophysical Journal International

Geophys. J. Int. (2013) **195,** 474–490
Advance Access publication 2013 July 5

doi: 10.1093/gji/ggt225

Optimization of a large-scale microseismic monitoring network in northern Switzerland

Toni Kraft,[1] Arnaud Mignan[1] and Domenico Giardini[2]

[1]*Swiss Seismological Service, ETH-Zurich, Switzerland. E-mail: kraft@sed.ethz.ch*
[2]*Institute of Geophysics, ETH-Zurich, Switzerland*

Accepted 2013 June 3. Received 2013 May 28; in original form 2011 November 14

SUMMARY

We have developed a network optimization method for regional-scale microseismic monitoring networks and applied it to optimize the densification of the existing seismic network in northeastern Switzerland. The new network will build the backbone of a 10-yr study on the neotectonic activity of this area that will help to better constrain the seismic hazard imposed on nuclear power plants and waste repository sites. This task defined the requirements regarding location precision (0.5 km in epicentre and 2 km in source depth) and detection capability [magnitude of completeness $M_c = 1.0$ (M_L)]. The goal of the optimization was to find the geometry and size of the network that met these requirements. Existing stations in Switzerland, Germany and Austria were considered in the optimization procedure.

We based the optimization on the simulated annealing approach proposed by Hardt & Scherbaum, which aims to minimize the volume of the error ellipsoid of the linearized earthquake location problem (*D*-criterion). We have extended their algorithm to:

(1) calculate traveltimes of seismic body waves using a finite difference ray tracer and the 3-D velocity model of Switzerland,

(2) calculate seismic body-wave amplitudes at arbitrary stations assuming the Brune source model and using scaling and attenuation relations recently derived for Switzerland, and

(3) estimate the noise level at arbitrary locations within Switzerland using a first-order ambient seismic noise model based on 14 land-use classes defined by the EU-project CORINE and open GIS data.

We calculated optimized geometries for networks with 10–35 added stations and tested the stability of the optimization result by repeated runs with changing initial conditions. Further, we estimated the attainable magnitude of completeness (M_c) for the different sized optimal networks using the Bayesian Magnitude of Completeness (BMC) method introduced by Mignan *et al.*

The algorithm developed in this study is also applicable to smaller optimization problems, for example, small local monitoring networks. Possible applications are volcano monitoring, the surveillance of induced seismicity associated with geotechnical operations and many more. Our algorithm is especially useful to optimize networks in populated areas with heterogeneous noise conditions and if complex velocity structures or existing stations have to be considered.

Key words: Seismic monitoring and test-ban treaty verification; Seismicity and tectonics.

1 MOTIVATION FOR MICROSEISMIC MONITORING IN NE SWITZERLAND

Seismic hazard assessment is an important component of the site safety evaluation for existing and newly planned nuclear power plants and radioactive waste repositories in Switzerland. Two components mainly contribute to seismic hazard in continental regions: the shaking hazard and the rupture hazard. The latter is dominated by small faults and fractures close to the infrastructure of interest that may remain undetected in standard site safety evaluations. A general need for a better assessment of existing fault networks in continental regions to improve seismic hazard estimates was recently expressed by England & Jackson (2011).

Passive microseismic monitoring is a tool to address this issue and has proven to be an invaluable tool for understanding underground processes since its inception in the 1970s (e.g. Lee & Stewart 1981; Bohnhoff *et al.* 2010). Yet, seismic network planning is still mainly performed as a manual task based on simple design rules, which cannot easily be transferred to complex cases. These design rules are, however, naturally solved in the framework of *D*-optimal network design (e.g. Steinberg & Rabinowitz 2003). Therefore, we used a simulated annealing approach (Kirkpatrick *et al.* 1983) to *D*-optimize microseismic network geometries for earthquake location at a regional scale. Based on the results of this analysis, we make recommendations for the size and geometry of such a network in NE Switzerland that is capable of locating earthquakes with a predefined precision and magnitude of completeness.

2 SEISMIC NETWORK OPTIMIZATION: METHOD

2.1 Synthetic earthquake catalogue and virtual station locations

Our study area was defined by the location of existing nuclear power plants and proposed nuclear waste repositories in Switzerland (Fig. 1). It extended from Lake Constance, in the northeast, to Lake Neuchâtel, in the southwest, and covered an area of about $200 \times 50\,\mathrm{km}^2$. Specifically, we defined the outline of the study area as follows. First, we added radial extensions of 25 km to the locations of the nuclear power plants and the contours of the planned radioactive waste repositories. Then, we constructed the convex hull around these extensions and two zones known to be seismically active (La Lance-Fribourg Zone in the southwest and Hegau-Bodensee Graben in the northeast; Fig. 1). With this step, we followed the recommendation of the International Atomic Energy Agency (IAEA) in Vienna (IAEA 2002):

> 3.9 Near regional studies should include a geographical area typically not less than 25 km in radius, although this dimension should be adjusted to reflect local conditions.

The perimeter defined by this procedure will be referred to as 'earthquake perimeter' and defines the area where the predefined requirements to the location precision and magnitude of completeness should be met.

For this region we generated a synthetic earthquake catalogue with a uniform distribution of epicentres and a depth distribution equal to the one observed for natural earthquakes in Switzerland (Giardini *et al.* 2004, Fig. 2). The magnitudes of the synthetic earthquakes—$M_\mathrm{L} \in [0.8 - 1.1]$—were chosen to cover a range around the desired magnitude of completeness $M_\mathrm{c} = 1.0$ (M_L), and to account for uncertainties in the determination of M_L. The magnitude–frequency distribution followed the Gutenberg–Richter relation (Gutenberg & Richter 1944):

$$\log(N) = a - bM, \tag{1}$$

where M is the magnitude, N is the cumulative number of events, a is the productivity of the observed volume and b is the relative earthquake size distribution. We found the values $a = 4.97$, $b = 1.17$, and $M_\mathrm{c} = 1.9$ (M_w) for the earthquake perimeter by applying the method of Wiemer & Wyss (2000) to the Earthquake Catalog of Switzerland (ECOS2002, Fäh *et al.* 2003). The total number of 2240 earthquakes in the resulting synthetic catalogue corresponded to a simulated period of 1 yr.

We also generated synthetic catalogues with fractal event distributions using a fractal dimension of $D = 1.3$. This value for the earthquake perimeter was found following the approach of

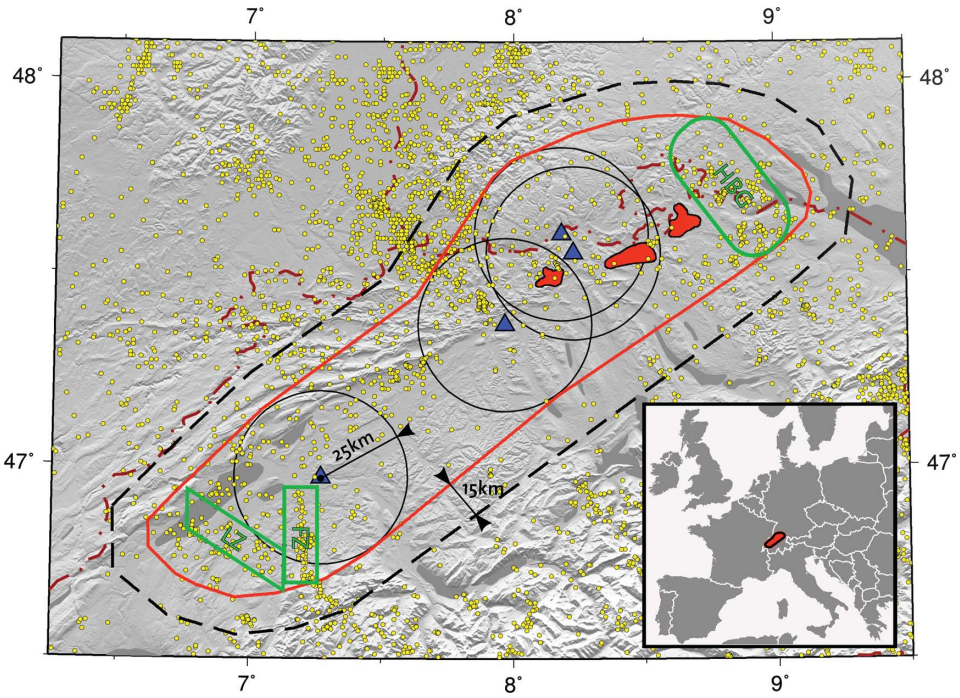

Figure 1. Map of the study area showing the earthquake perimeter (solid red line) and station perimeter (dashed black line) used for the network optimization. Nuclear power plants are indicated by blue triangles and are surrounded by circles of 25 km radius. Sites of proposed radioactive waste repositories are shown as red areas. Earthquakes from 1975 to 2008 from the ECOS2009 catalogue (Fäh *et al.* 2011) are plotted as yellow dots. Green polygons indicate seismic active zones that were included in the study area (LZ, La Lance Zone; FZ, Fribourg Zone; HBG, Hegau-Bodensee-Graben). Inset: map of Central Europe with study area indicated in red.

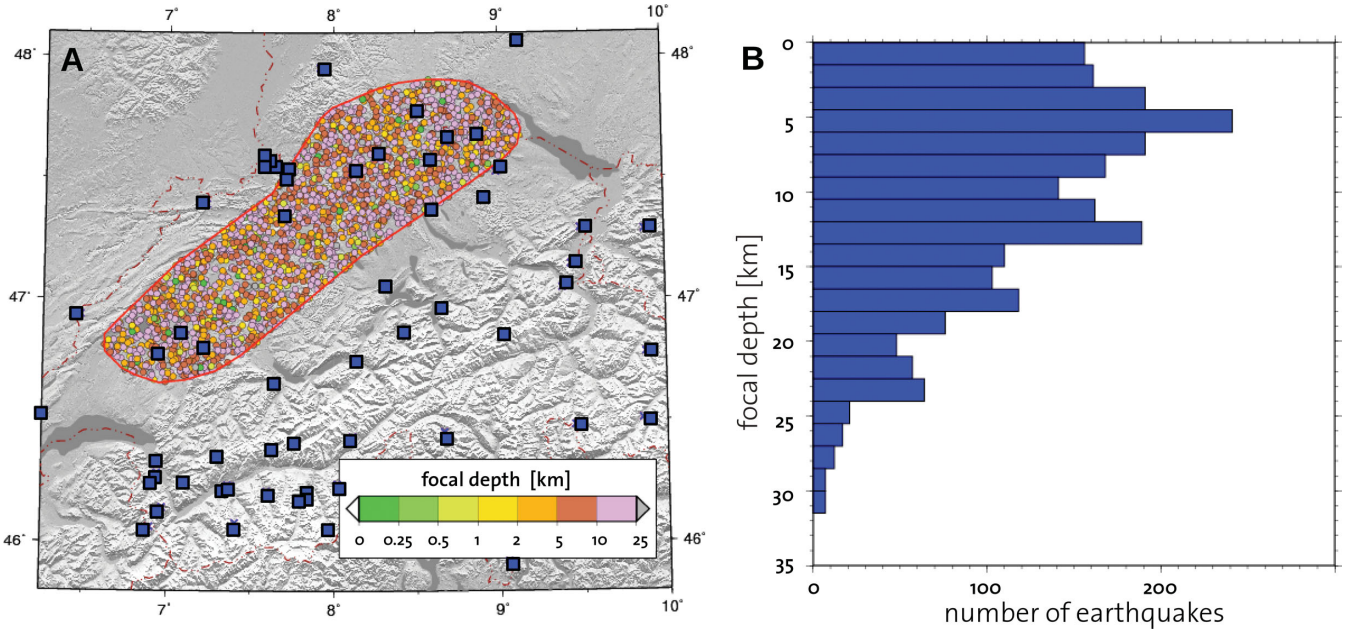

Figure 2. (A) Map of the study area showing the synthetic earthquake catalogue used for the network optimization. Colour scale indicates source depth. Red polygon shows the earthquake perimeter. Blue squares show the used existing stations in Switzerland, Germany and Austria. (B) Depth distribution of the synthetic earthquakes in the catalogue using a binning interval of 1.5 km. The distribution corresponds to the earthquake depth distribution observed in Switzerland (Giardini *et al.* 2004).

Grassberger & Procaccia (1983), and using the ECOS2002 catalogue (Fäh *et al.* 2003). However, the fractal catalogues did show a very strong clustering along linear structures, and we excluded them from further analysis, in order not to bias the network optimization towards unrealistic features in the synthetic catalogue.

The geographical region for possible new station locations ('station perimeter') was derived by enlarging the earthquake perimeter by 15 km (Fig. 1). This step was motivated by the empirical design rule that a seismic network should enclose the source region of interest. The station perimeter was then filled by a triangular grid with mean spacing of 4.5 km using an open-source mesh generator (Persson & Strang 2004). Each of the 952 nodes of the grid represented a potential location for a seismological station of the new network (Fig. 3). In the following, we will call these locations 'virtual stations'. The appropriate altitudes for the virtual stations were taken from the digital elevation model of the Shuttle Radar Topography Mission (Farr *et al.* 2007).

In our optimization, we considered all existing stations that were transmitting data to the Swiss Seismological Service (SED) in real-time and were routinely used for earthquake location in 2010. This means that if the ratio between the calculated body-wave amplitude of a synthetic earthquake and the observed noise level at any of these stations was equal or lager than ten, the contribution of that station to the location of the synthetic earthquake was considered in the optimization process. These stations included 64 of the Swiss national seismic network, two of the Landesamt für Geologie, Rohstoffe und Bergbau im Regierungspräsidium Freiburg, Baden-Württemberg (LGBR), Germany, and one of the Zentralanstalt für Meteorologie und Geophysik (ZAMG), Austria.

2.2 First-order ambient noise model for Switzerland

To estimate the expected noise levels at the virtual stations, we developed a first-order ambient noise model for Switzerland and surrounding regions. The model was derived from high-resolution (250 m × 250 m) land-use data of Europe compiled by the European Commission project CORINE (Büttner *et al.* 2004) using satellite images. We decomposed the Swiss CORINE data into 13 separate grids corresponding to the land-use classes indicated in Table 1 and Fig. 4. Additionally, a grid with georeferenced information on highways and main roads (source: Swiss Federal Statistical Office 2011) was generated. Then we multiplied the 14 land-use grids by unit-free noise weights, which are documented in Table 1. The weighting scheme was solely based on experience-guided expert judgment. To account for noise propagation away from its sources, the land-use grids for industrial areas, mines, urban zones and highways, and main roads, were smoothed using a Gaussian filter with a width of 2.5 km. All land-use grids were merged into one final grid by assigning the maximum value reached in a pixel in all 14 land-use grids to the corresponding pixel in the final grid. The resulting grid represents a first-order ambient noise model of Switzerland and surrounding regions and is shown in Fig. 5.

In this study, we associated each noise class (Table 1) with a noise level corresponding to the rms ground velocity in the frequency range of 1–10 Hz. Using the software PQLX (McNamara & Boaz 2005), we computed probability density functions of the power spectral density (PSDPDF) for the ground acceleration recorded at the existing stations in 2010. Then, we derived the mode function, P_a, of the PSDPDF for each station. The mode function represents the most probable noise level observed at the corresponding station for the analysed time window. The mean value of the ground-velocity-converted mode function, $\langle P_a/\omega^2 \rangle$, over the frequency range $f \in [f_1, f_2]$ can be related to the rms ground velocity amplitude, v_{rms}, in the same frequency range by (Bormann 1998):

$$v_{rms} \approx \sqrt{2 \cdot \langle P_a/\omega^2 \rangle \cdot (f_2 - f_1)}, \quad (2)$$

where ω represents the angular frequency.

By comparing the so derived rms ground velocities to the noise classes predicted by the ambient noise model for the existing

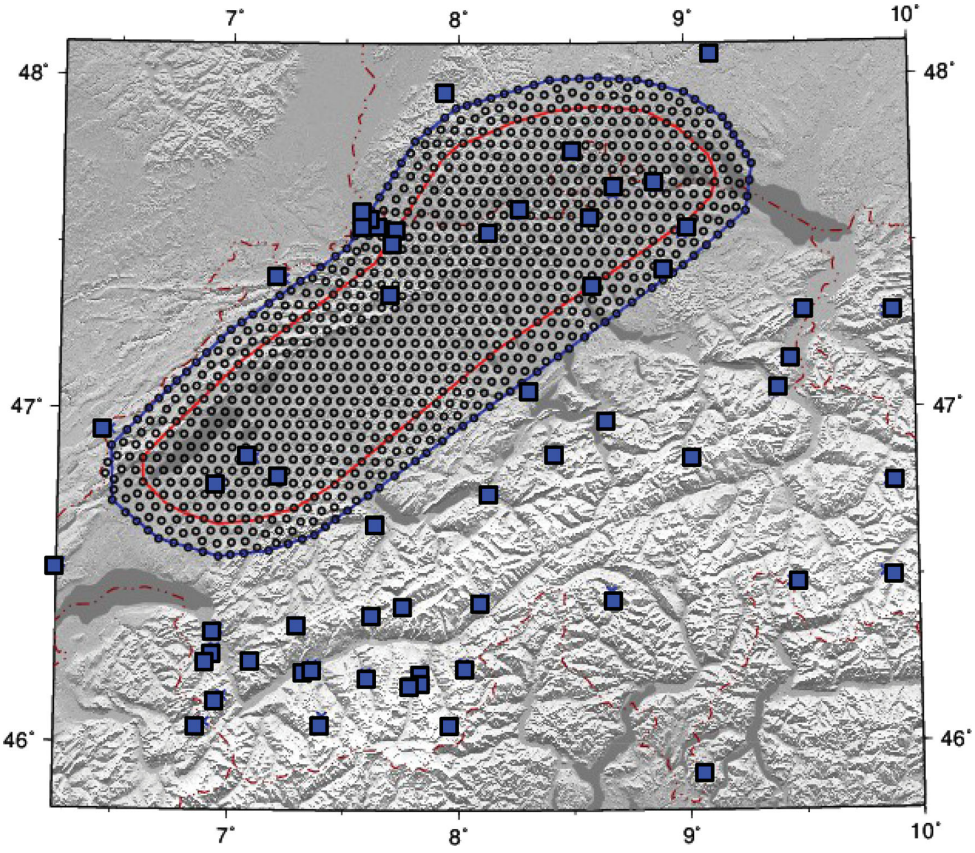

Figure 3. Map of 952 possible locations of new (black circles) and existing (blue squares) seismological stations used for the optimization. Red and blue polygons show the earthquake and station perimeter, respectively.

Table 1. Noise level classification of the 13 land-use classes of the CORINE project and one from open GIS data (Fig. 4) into three noise classes. The classification was solely based on experience-guided expert judgment. Unit-free noise weights larger than 90 correspond to noise class High. Noise weights smaller than 35 are associated with noise class Low. Asterisk indicates the application of Gaussian smoothing (see text).

CORINE land-use class	Noise class	Noise weight
Industrial, commercial and transport	High	150*
Mine, dump or construction sites	High	120*
Urban fabric	High	100*
Artificial vegetated areas, non-agricultural	Middle	50
Arable land	Middle	50
Agricultural areas, heterogeneous	Middle	50
Permanent corps	Middle	40
Forests	Middle	40
Pastures	Low	20
Shrub; herbaceous vegetation	Low	20
Open spaces w. little vegetation	Low	20
Inland wetlands	High	255
Inland water	High	255
Additional noise sources	**Noise class**	**Noise weight**
Highways and main roads	High	150*

stations, we were able to define v_{rms} bounds for each noise class: Low: $v_{\mathrm{rms}} \leq 30\,\mathrm{nm\,s^{-1}}$, High: $v_{\mathrm{rms}} > 120\,\mathrm{nm\,s^{-1}}$ and Middle: v_{rms} in between these values. Based on this analysis, we assigned the following synthetic noise levels to the virtual stations depending on the noise class derived from the first-order noise model: $v_{\mathrm{rms}} = 15\,\mathrm{nm\,s^{-1}}$ (Low), $v_{\mathrm{rms}} = 60\,\mathrm{nm\,s^{-1}}$ (Middle) and $v_{\mathrm{rms}} = 139\,\mathrm{nm\,s^{-1}}$ (High).

Fig. 6 illustrates the generally good agreement of the noise classifications based on instrumental recordings and the first-order model. The majority of stations with high or low instrumental noise were assigned to the equivalent class of the noise model. Only for noise class Middle the model seems to be slightly biased towards optimistic estimates (Fig. 6). Considering, however, that the noise model does not account for effects of the local geology and does not consider noise level variations within the individual land-use classes, misclassifications are to be expected.

2.3 Calculation of synthetic body wave amplitudes

We have chosen a signal-to-noise ratio (SNR) of 10 as the threshold for an earthquake to be observed at a certain station. The SNR was defined as the ratio of the synthetic amplitude of the body wave under consideration and the observed or estimated v_{rms} noise level at the station (see previous section). In general, an SNR ≥ 3 is considered being sufficient to reliably determine a seismic phase onset in a seismogram (e.g. Hardt & Scherbaum 1994). However, our estimate of the signal amplitude corresponds to the maximum expected amplitude of the considered body wave at the recording station, which may be significantly larger than the amplitude of the phase onset. Moreover, the geology at the recording station does not necessarily agree with the hard rock conditions assumed in the computation of synthetic body wave amplitudes. To account for these uncertainties, we decided to use a more conservative SNR threshold.

The amplitude of a seismic phase is influenced by two major factors: the earthquake source process and wave propagation effects.

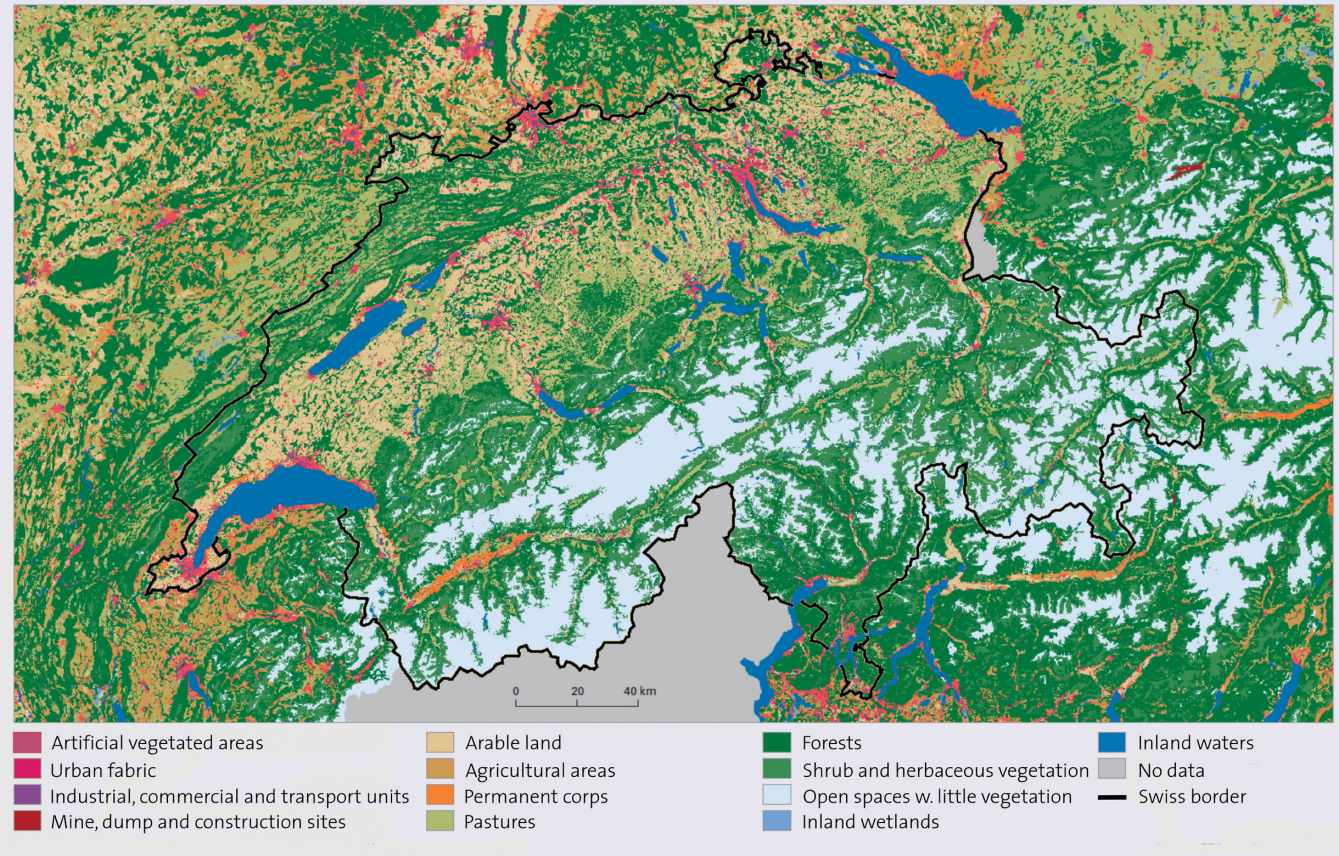

Figure 4. Land-use map of Switzerland and surrounding regions derived by the CORINE project (Büttner *et al.* 2004). The 13 land-use classes have a resolution of 250 m × 250 m and are indicated with their colour code at the bottom. (Modified from: Swiss Federal Statistical Office 2011)

Both effects were only treated in an approximate way in this study. Especially, path effects were treated to only result from geometrical spreading, constant-Q attenuation (Bay *et al.* 2003, 2005) and free-surface amplification (Müller 1986). For the seismic source we assumed the Brune model (Brune 1970, 1971). Input parameters for the source model were derived from scaling relations for local magnitude (M_L) to seismic moment (Edwards *et al.* 2010) and moment magnitude to stress drop (Bay *et al.* 2003, 2005) that were recently derived for Switzerland. Considering that available focal mechanisms for the study area are rather heterogeneous and cover mainly magnitudes above $M_L = 2.5$ (Kastrup *et al.* 2004), we decided not to account for the radiation patterns of the synthetic earthquakes but only to use their individual integral averages (Aki & Richards 1980).

In Fig. 7(A) calculated *P*-wave amplitudes are plotted as a function of ray length for all earthquakes of the synthetic catalogue used in the optimization procedure. The figure indicates that stations with high, intermediate or low noise levels should record *P* waves of the synthetic earthquakes up to distances of around 5, 30 or 100 km, respectively. Therefore, a network of stations that are mainly classified as belonging to the noise classes Middle and Low, like the Swiss Digital Seismic Network (SDSNet; see Fig. 10A), is expected to record *P* waves of M_L 1 earthquakes up to distances between 30 and 100 km, with a maximum between these values, and a decreasing number of observations towards the higher threshold. Such a distribution is actually observed for M_L 1 earthquakes recorded on the SDSNet (Fig. 7B). Therefore, we are confident that our model is able to reliably predict the detectability of seismic body waves at a given station.

2.4 Network optimization criterion: *D*-optimality

Seismic network optimization is a special case of optimal experimental design that aims to identify network geometries that are optimal with respect to some statistical criterion. Our approach is based on minimizing the volume of the confidence ellipsoid of the earthquake location (Kijko 1977). The approximate covariance matrix of the linearized earthquake location problem can be described as (Menke 1989):

$$\mathrm{cov(m)} = \sigma^2 \left(G^T G\right)^{-1}, \tag{3}$$

where m is the vector of hypocentral parameters (x, y, z, origin time to), σ^2 is the variance of uncertainties in arrival-time determination and G is the matrix of partial derivatives with respect to hypocentral parameters.

We computed the partial derivatives in G by posterior ray tracing in 3-D traveltime fields using the steepest gradient algorithm of Benz *et al.* (1996). The traveltime fields were calculated by applying the finite-difference ray tracer of Podvin & Lecomte (1991) to the Swiss 3-D *P*-wave velocity model (Husen *et al.* 2003). The partial derivatives were then approximated by difference quotients calculated from the appropriate endpoint coordinates of the first ray-segment leaving the hypocentre.

The shape of the confidence ellipsoid can be described by the eigenvalues and eigenvectors of $(G^TG)^{-1}$ and its volume is proportional to $1/\det(G^TG)$ (Flinn 1965; Buland 1976). If the determinant $\det(G^TG)$ is used as an optimization measure, the corresponding optimization criterion is known as the '*D*-criterion' (Kijko

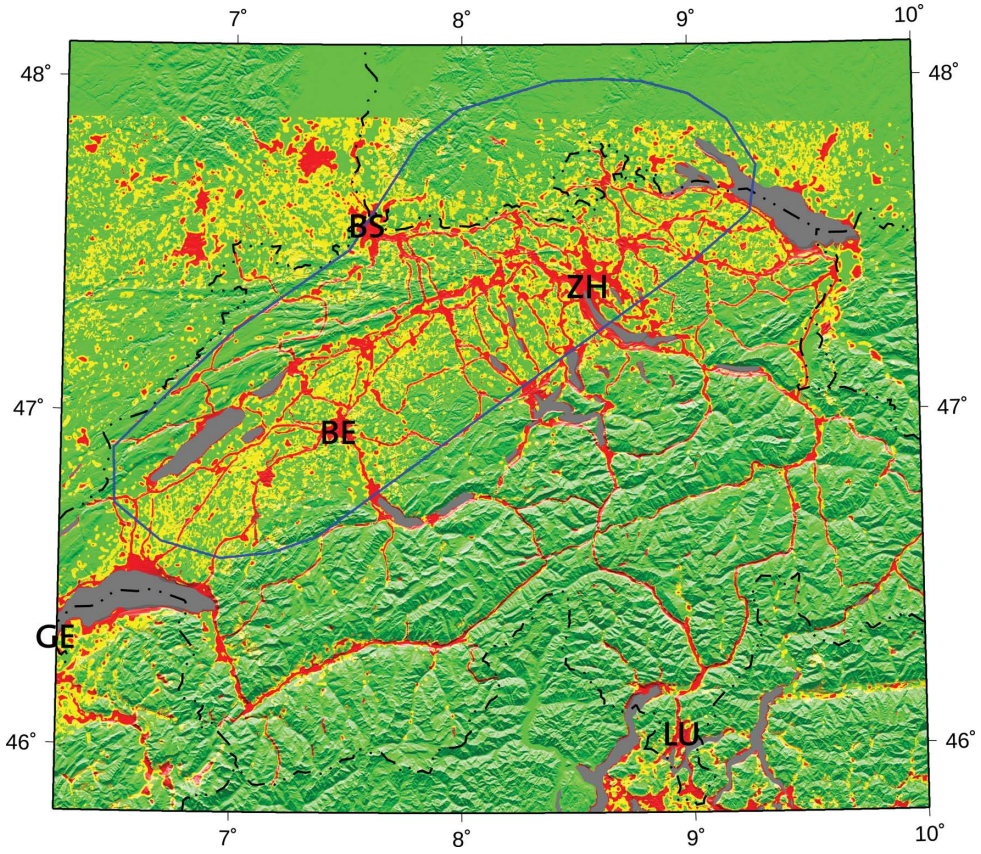

Figure 5. First-order ambient noise model of Switzerland and surrounding regions derived from CORINE land-use data. Colours indicate the resulting noise classes (ground velocities) that were assigned to virtual stations at the corresponding locations [red: High (139 nm s^{-1}); yellow: Middle (60 nm s^{-1}), green: Low (15 nm s^{-1})]. The blue polygon indicates the station perimeter used for the optimization. No land-use data were available for latitudes larger than 47.86° (CHy > 303 610), for Lichtenstein, and parts of Italy. For these areas a noise level of 30 nm s^{-1}, which separates noise classes Low and Middle, was used. Some large cities are indicated (BE, Bern; ZH, Zurich; BS, Basel; GE, Geneve; LU, Lugano).

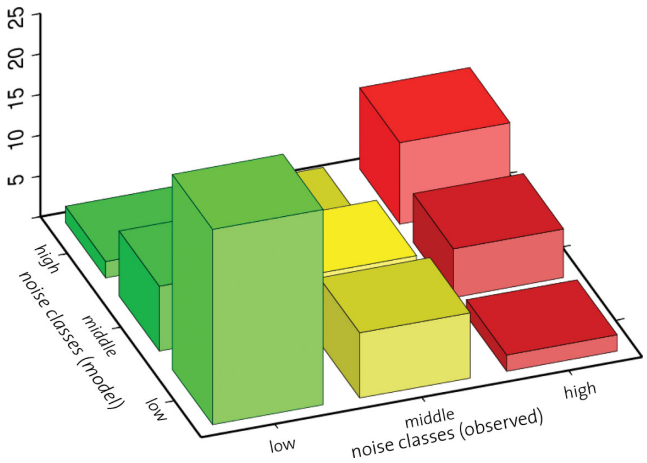

Figure 6. Histogram comparing the noise level classification for the existing stations according to observation and derived from the first-order noise model, respectively. The stations are mainly grouped in equal noise classes in both cases, which demonstrates the generally good agreement of ambient noise model and noise measurements at existing stations.

1977), and the resulting optimal experimental design is referred to as '*D*-optimal'.

The *D*-criterion for one earthquake can be generalized to the case of *N* earthquakes by defining the measure (e.g. Rabinowitz & Steinberg 1990):

$$D = \sum_{i=1}^{N} \alpha_i \log\left(\det\left(G_i^T G_i\right)\right), \tag{4}$$

where the index i indicates the earthquake and α_i is its individual weight. In this study we did not weight individual events, and set $\alpha_i = 1$.

D-optimal network design has been frequently used in seismological research to evaluate the properties of particular simple networks (e.g. Peters & Crosson 1972; Minster *et al.* 1974; Lilwall & Francis 1978; Uhrhammer 1980; Satake 1985; Souriau & Woodhouse 1985), whereas, in practice, seismic network design is still largely left to professional intuition based on empirical design rules. These design rules are, however, easily and naturally solved in the framework of *D*-optimal design (e.g. Steinberg & Rabinowitz 2003).

Only few researchers have so far addressed the problem of non-detections in the optimization process (e.g. Hardt & Scherbaum 1994; Zayats & Steinberg 2010). Non-detections generally occur if the amplitude or frequency of the seismic signal to be detected at a station does not change by a significantly enough amount with respect to the background noise. As described earlier, we developed a model to predict the detectability of seismic body waves at arbitrary locations in Switzerland. Our model did not account for detections based on a pure frequency change. Yet, we are working on incorporating this aspect into our algorithm in the future (Goertz *et al.* 2012). We used our model to decide whether a station–event

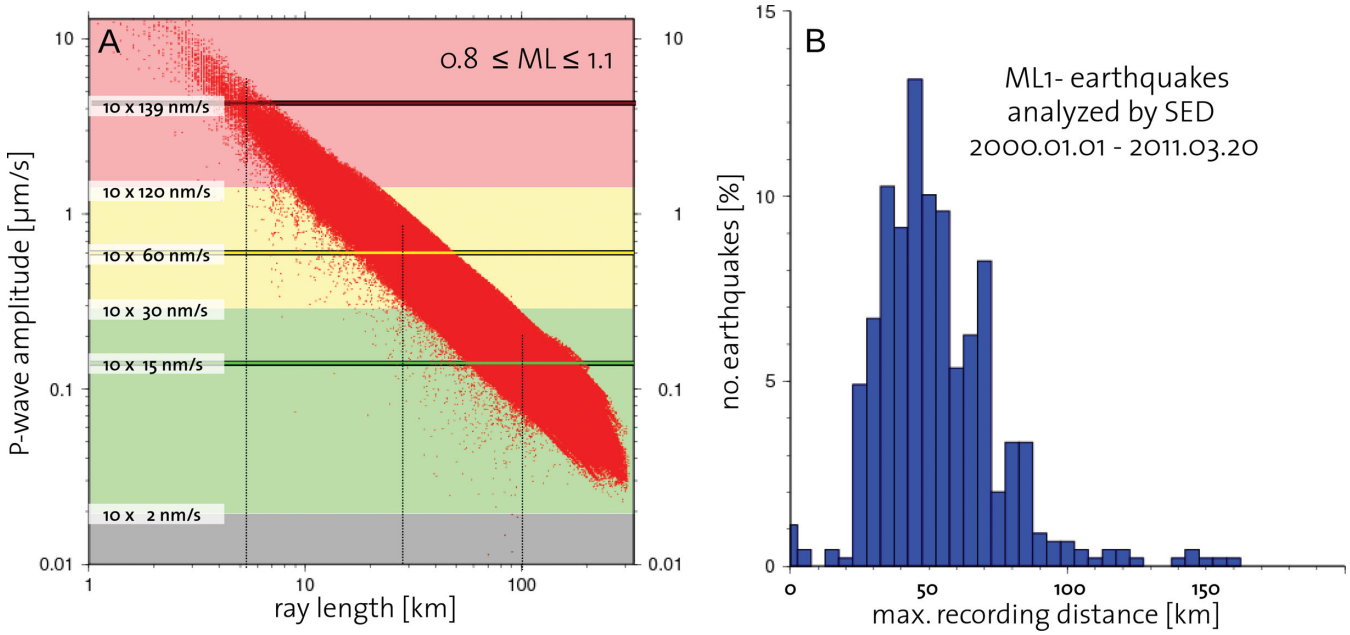

Figure 7. (A) Synthetic *P*-wave amplitudes of earthquakes used for the optimization (red). Background colours illustrate the range of the noise classes (grey: typical resolution of short period seismometer). The noise levels assigned to virtual stations of a corresponding class were multiplied by a factor of 10 to account for the detection threshold (SNR $\geq$10), and are indicated as horizontal lines. Dashed vertical lines indicate the expected maximum observation distance for $M_L \sim 1.0$ earthquakes in the corresponding noise class. (B) Histogram of maximum observation distances for *P* waves of M_L 1 earthquakes recorded in Switzerland. [Max. epicentral distance of *P* arrival listed in SED earthquake database for the time period of 2000 Jan to 2011 March; $M_L = 0.8$–1.1)].

pair (observation) is considered in the network optimization or not. Adapting the detection criterion implemented in the automatic earthquake analysis system of the SED, we did not consider earthquakes with less than four *P*-wave observations in the optimization process.

2.5 Network optimization approach: simulated annealing

A general problem in optimization is the large size of the solution space that has to be searched to find the optimal solution. As pointed out by Bartal *et al.* (2000), the number of all possible configurations of a network consisting of *N* stations positioned on a grid of *M* points without repetition is given by:

$$\binom{M}{N} = \frac{M!}{N!\,(M-N)!}. \tag{5}$$

For a small problem with six stations on a 6×6 grid, this amounts to 1 947 792 combinations, where no distinction between geophysical meaningful or meaningless geometries is made. In the case of this study, with $M = 952$ and $N = 10$, 15, 18, 20, 22, 24, 26, 28, 30 and 35, the number of possible combinations lies between 10^{23} ($N = 10$) and 10^{63} ($N = 35$), which does not allow to solve these optimization problems in a brute force approach, that is, by testing all possible network configurations. This is why we used a simulated annealing algorithm to solve our optimization problem (Hardt & Scherbaum 1994).

Simulated annealing (Kirkpatrick *et al.* 1983) replicates a concept of material science involving heating and controlled cooling of a material to increase the size of its crystals and to reduce their defects. In simulated annealing a synthetic temperature, *T*, is lowered according to a predefined annealing schedule. Its functional form depends on the optimization problem under consideration and has to be adjusted beforehand (Basu & Frazer 1990). In this study, we used the following annealing schedule, which was found by trial and error:

$$T_n = T_0 \cdot \left(1 - \frac{n}{N}\right)^6. \tag{6}$$

In eq. (6), T_0 is the starting temperature and T_n is the temperature at time step $n \in [0, N]$, with $N = 1000$.

The quality of the solution is described by the cost function, *C*, which corresponds to the free energy in the case of annealing a metal. In this study, we have implemented a cost function for the earthquake location problem of the form $C = 1/D$, with *D* as defined in eq. (4). In general, it is possible to combine more than one cost function and to optimize a problem in terms of several constraints (e.g. Hardt & Scherbaum 1994).

During the optimization process, many random solutions—in our case 200 network configurations—are tested at every temperature step. This number was again chosen by trial and error to achieve a slow and smooth convergence of the solution to the global minimum (Fig. 8). Solutions that do not lower the cost function, called poor solutions, are accepted if the following criterion is satisfied (Metropolis *et al.* 1953):

$$\exp(-\Delta C/T) > \mathrm{rand}(0,1), \tag{7}$$

where *T* is the synthetic temperature, rand(0, 1) is a random number in the interval [0, 1] and ΔC (negative for a good; positive for a poor solution) is the difference of the cost function in the current solution and the currently accepted solution, that is, the 'winner' solution of the last temperature step. If *T* in eq. (7) is large, many poor solutions are accepted and a large part of the solution space is explored. The advantage of this procedure is that local minima in the solution space can be overcome and a global minimum can be found. Fig. 8 illustrates a typical optimization run. At high synthetic temperatures, the value of the cost function of the winner and overall best solution deviate strongly. When the synthetic

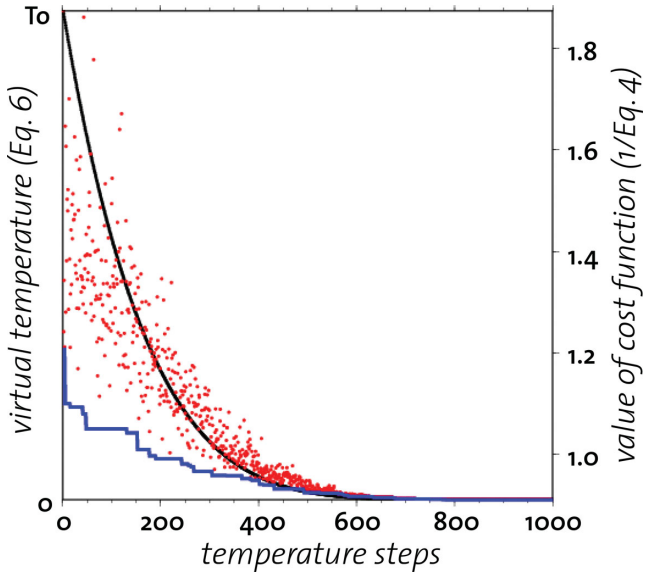

Figure 8. Illustration of the simulated annealing algorithm. The annealing schedule for the synthetic temperature T (black, Eq. 6) and the value of the cost function (Eq. 4) of the currently accepted solution (winner, red) and overall best solution (blue) are shown. For details refer to the text.

temperature is decreased following the annealing schedule, the value of the cost function of the winner solution converges towards the overall best solution, and the value of the cost function of the overall best solution constantly decreases and converges towards the optimal solution.

3 SEISMIC NETWORK OPTIMIZATION: APPLICATIONS

In the following we will apply our algorithm to optimize seismological network geometries. We will start by briefly discussing optimization results for simple test cases to validate the performance of our algorithm. We will then apply our algorithm to optimize a regional-scale microseismic network in northern Switzerland.

3.1 Simple test cases

In the following four test cases described, we have used a homogenous velocity model with a constant P-wave velocity of 6 km s^{-1}. The geometry of the virtual station grid had a similar geometry as the one used in the optimization for northern Switzerland described in the next section (Fig. 9). All parameters of the virtual stations were identically chosen to the Swiss case. Specifically, in test cases B and D we used the noise levels derived from the first-order ambient noise model described earlier. In each case we optimized a network of four new stations that extended an existing network of 22 stations. The locations of these new stations were optimized with respect to one or two M_L 1 earthquakes, respectively.

Test case A: One single M_L 1 earthquake was located at 5 km depth. All stations (26) had the same noise level of 60 nm s^{-1} (noise class Middle). The earthquake was not recorded at any of the 22 existing stations. Therefore, the case could be interpreted as optimization for a simple four-station network. The resulting station geometry represents the well-known triangular quadripartite network (Uhrhammer 1980), with one station as close as possible to the epicentre and three stations equally spaced on a circle centred on the epicentre (Fig. 9A). The radius of the circle was determined by the largest epicentral distance that allowed the detection of the earthquake (SNR $\geq$ 10).

Test case B: The noise level assumed for all stations was derived from the first-order ambient noise model, described in Section 2.2. All other parameters were identical to test case A. The M_L 1 earthquake was in general detected at larger distances than in test case A. Yet, depending on the noise level, several stations close to the epicentre did not detect the earthquake. Again, the resulting optimal network represented a variant of the triangular quadripartite network (Fig. 9B). However, the radius of the outer circle of stations was significantly larger than in test case A. Two stations of the existing network in the southeast of the epicentre detected the earthquake and constrained the geometry of the triangular network. Two of the new stations were placed on the northwestern rim of the station perimeter. The two remaining stations were sited close to each other near the epicentre. These closely spaced stations mainly generate redundant information; hence, one of them may not be needed. Yet, by placing this additional station close to the most important station in the centre of the network (Steinberg & Rabinowitz 2003), the cost function could efficiently be further reduced. We interpret the station clustering in the D-optimal network solution as a weight of the importance of a station location and will make use of this feature in the subsequent analysis (see Discussion).

Test case C: All parameters were chosen identical to test case A. Yet, an additional M_L 1 earthquake was introduced at 5 km depth in the eastern part of the study area (Fig. 9C). The two earthquakes had largely separated detection areas that overlapped only in a small region. The newly added eastern earthquake was recorded at several existing stations, which could, therefore, contribute to the solution of the location problem. The geometry of these stations was already close to a triangular quadripartite network. Hence, the optimization concentrated mainly on the western earthquake, and the result was very similar to test case A. In test case C, however, the triangular quadripartite network centred on the western earthquake was rotated in a way that one station on the outer circle was placed in the overlapping region of the detection areas of the two earthquakes (Fig. 9C). The rotation of the network did not change the location uncertainties for the first earthquake but ensured that the above-mentioned station could contribute to the location of both earthquakes. In that way, the overall cost function could be further decreased and approached its global minimum.

Test Case D: Here, we used the same parameters as in test case B but considered the two earthquakes described in test case C. Both earthquakes were recorded at existing stations (Fig. 9D). Yet, the number of stations recording the eastern event was larger, and their geometry had a better azimuthal coverage than that of stations recording the western earthquake. The optimization result was identical to that of test case B. Considering the nearly optimal geometry of the existing stations that recorded the eastern earthquake, it is obvious that the optimization had to focus on the western event to effectively reduce the value of the cost function.

In summary, the optimization results for the discussed test cases show that our optimization algorithm is able to:

(1) find D-optimal networks that agree with theoretical considerations and results of other researchers (e.g. Steinberg & Rabinowitz (2003) and references therein),

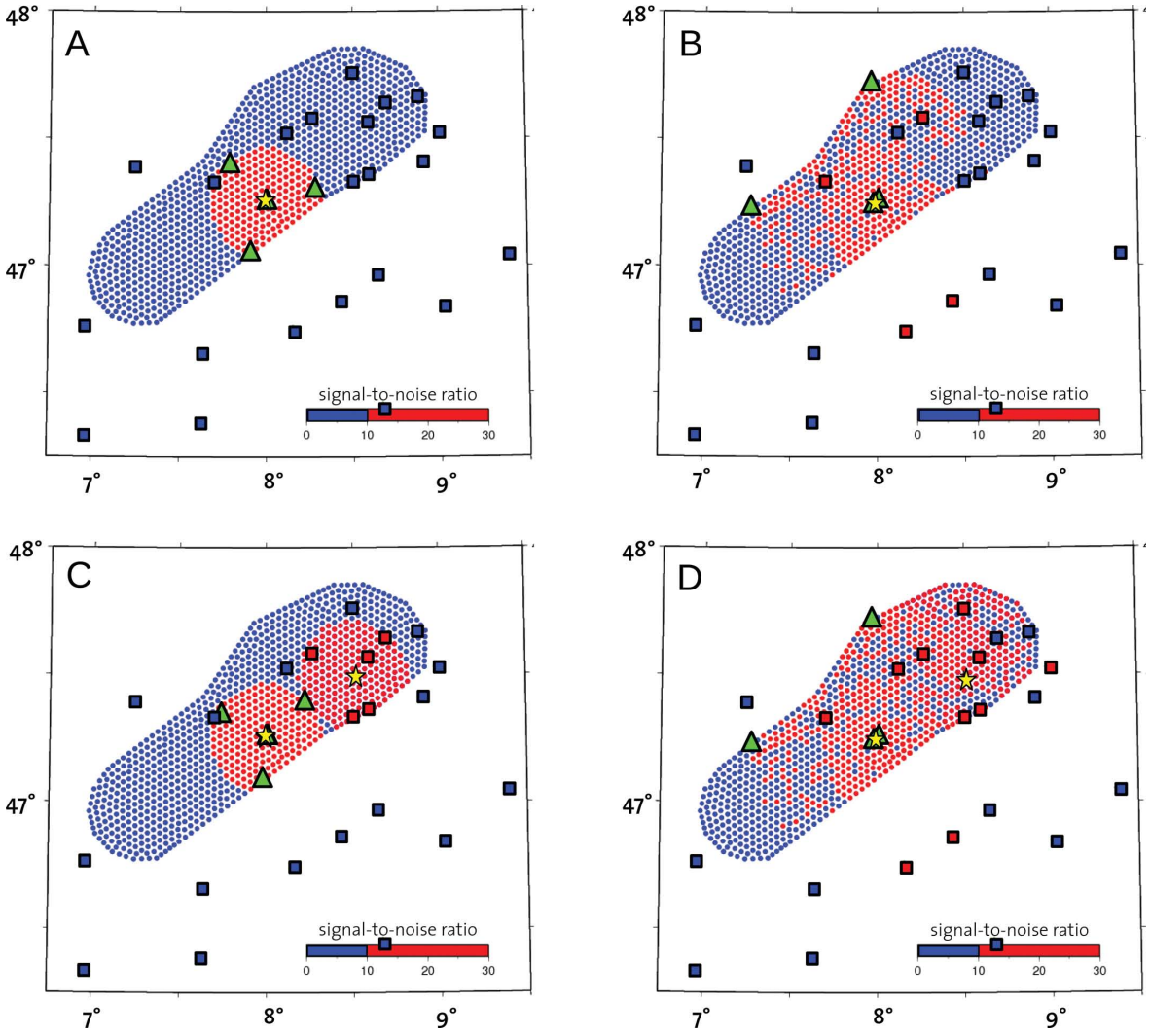

Figure 9. Optimization results for simple test cases, with networks consisting of 22 existing and four new stations. Either one (A,B) or two (C,D) M_L 1 earthquakes at a depth of 5 km are considered in each case. Earthquake locations are indicated by yellow stars. Existing stations are indicated by coloured squares, virtual stations by coloured dots. The colour code indicates if the earthquakes are detected (red) or missed (blue) at a site. Green triangles indicate the *D*-optimal geometry of the four station networks. Station noise level considered is either middle [60 nm s^{-1}; A, C) or corresponds to the noise-levels taken from the first-order ambient noise model derived in this study (B, D).

(2) correctly consider varying station noise levels and
(3) correctly handle multiple event setups.

3.2 Regional-scale microseismic network, NE Switzerland

We applied our optimization algorithm to find *D*-optimal network geometries for a regional-scale microseismic network in northern Switzerland. The goal of the optimization was to determine the size and geometry of a seismological network that ensured a location precision of 0.5 km in the epicentre and 2 km in source depth, as well as a magnitude of completeness of $M_c = 1$ (M_L) in the area defined by the earthquake perimeter in Section 2. The input parameters to the optimization were as follows:

(1) An existing network of 67 stations in Switzerland, Germany and Austria (Fig. 4). The observed noise levels of the individual stations were taken into account (Fig. 10A).

(2) A grid of 952 virtual stations (Fig. 3) with noise levels taken from the first-order ambient noise model for Switzerland and surrounding regions (Fig. 5).

(3) A synthetic earthquake catalogue including 2240 events in the magnitude range $M_L = 0.8$–1.1 (Fig. 2).

(4) Networks with $N = 10$, 15, 18, 20, 22, 24, 26, 28, 30 and 35 stations were tested.

The predicted observation rate at a site, that is, the percentage of observed catalogue events (Fig. 10B), is of considerable interest for the interpretation of the optimization results. As can be inferred from Fig. 10(B), the predicted observation rates found in this study were functions of the epicentral distance to, and the noise-level at, a given site. A high detection rate (>50 per cent) was generally predicted for stations with noise class Low at epicentral distances less than 100 km, whereas, the predicted observation rates for stations with noise class Middle or High were only low (<30 per cent) even if the stations were located inside or close to the earthquake perimeter (Fig. 10B). This general trend was observed for existing and virtual stations.

Two other patterns could be identified in the predicted observation rates for the virtual stations. First, the detection rates were generally smaller at the eastern and western edges of the station perimeter

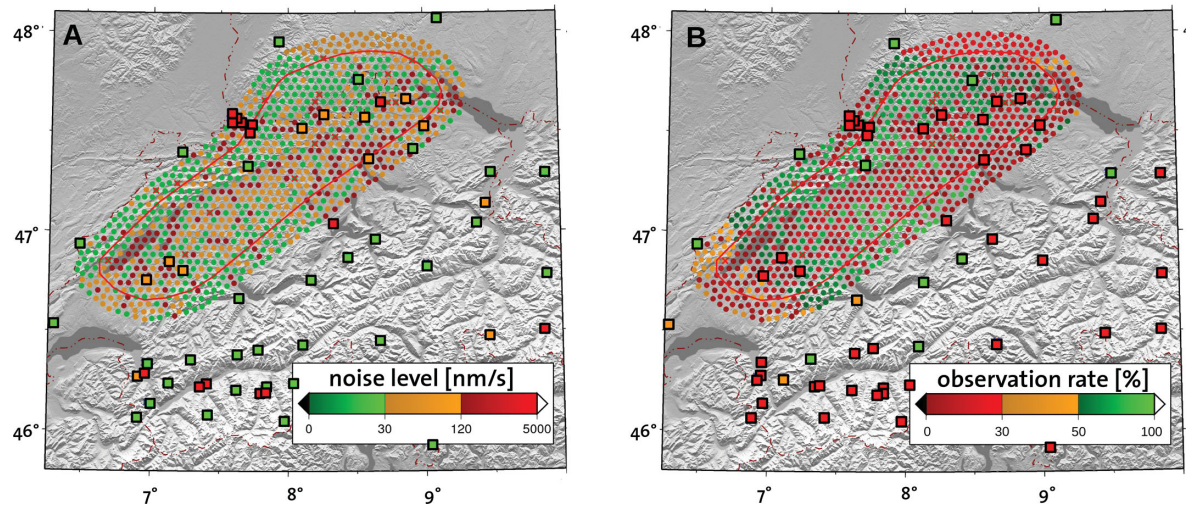

Figure 10. (A) Noise levels observed at the existing stations (squares) and predicted for the virtual stations (dots). (B) Predicted observation rates for the 2240 synthetic earthquakes at the existing (squares) and virtual (dots) stations. The earthquake perimeter is indicated in (A) and (B) as a red polygon.

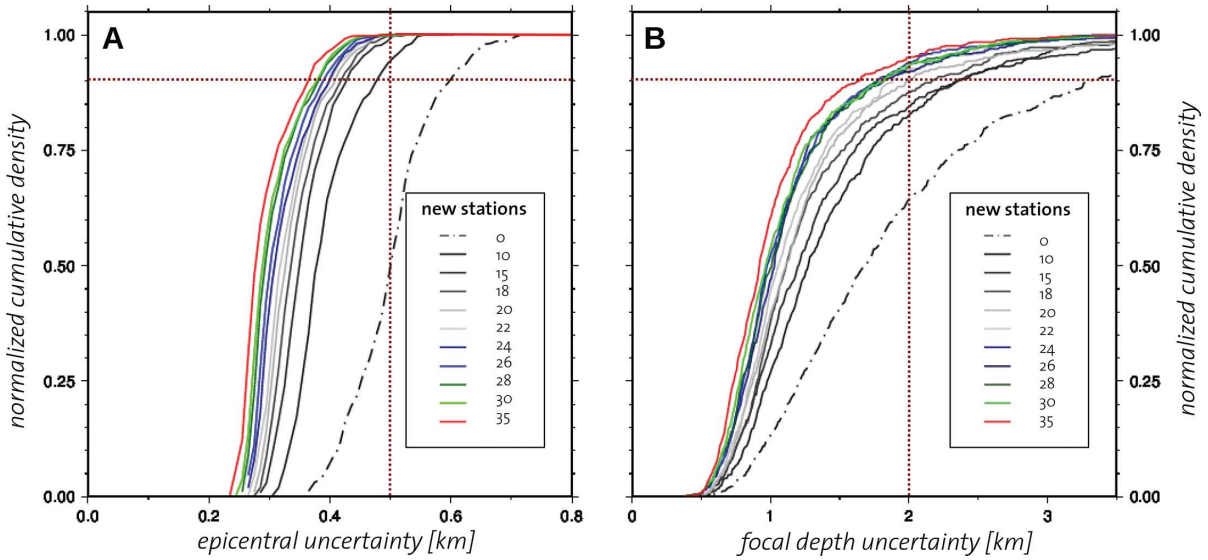

Figure 11. Normalized cumulative density functions (nCDF) of 2σ epicentral and focal depth errors for the 2240 synthetic earthquakes in the earthquake perimeter for networks with 0–35 new and the existing stations. Dashed red lines indicate the 90 per cent level and the desired uncertainties, respectively.

than in the centre of this region (Fig. 10B). This can be explained by a simple geometrical effect governed by epicentral distance that caused stations at the eastern edge of the perimeter to have a small probability to detect earthquakes at the western edge of the perimeter and vice versa. For the same reason, stations in the centre of the perimeter had a high probability to detect earthquakes at the eastern and western edges and yielded higher total observation rates.

Secondly, stations at the western end of the station perimeter had slightly lower predicted observation rates than their counterparts in the east. This observation can be explained by the larger size of the eastern side of the station perimeter, which, due to this fact, contained more synthetic earthquakes. In addition, owed to the higher population density in the western part of the study region, the predicted noise levels were in general higher than in the eastern part, where the first-order ambient noise model contains large low-noise areas (e.g. Black Forest, Fig. 10A).

We assessed the performance of the different networks with respect to errors in epicentre and focal depth by calculating normalized cumulative density functions (nCDF) of the epicentral (σ_h) and depth (σ_z) uncertainties at the 2σ level for all 2240 synthetic earthquakes (Fig. 11). For a given uncertainty, these functions show the fraction of the synthetic earthquakes that had location uncertainties equal to or smaller than the given one. The epicentral errors (σ_h) were calculated from the geometric mean of the uncertainties of the epicentral coordinates (σ_x;σ_y) by:

$$\sigma_h = \sqrt{\sigma_x \cdot \sigma_y \cdot \Delta\chi^2}; \quad \Delta\chi^2 = 6.17, \tag{8}$$

where $\Delta\chi^2$ accounts for the increase in the degree of freedom (Press *et al.* 1992).

The uncertainties of the individual hypocentre coordinates were estimated by means of the covariance matrix of the scatter density cloud derived from the posterior probability density function (PDF) for the earthquake location problem (Lomax *et al.* 2000). The posterior PDF represents a complete probabilistic solution to the location problem, including information on uncertainty and

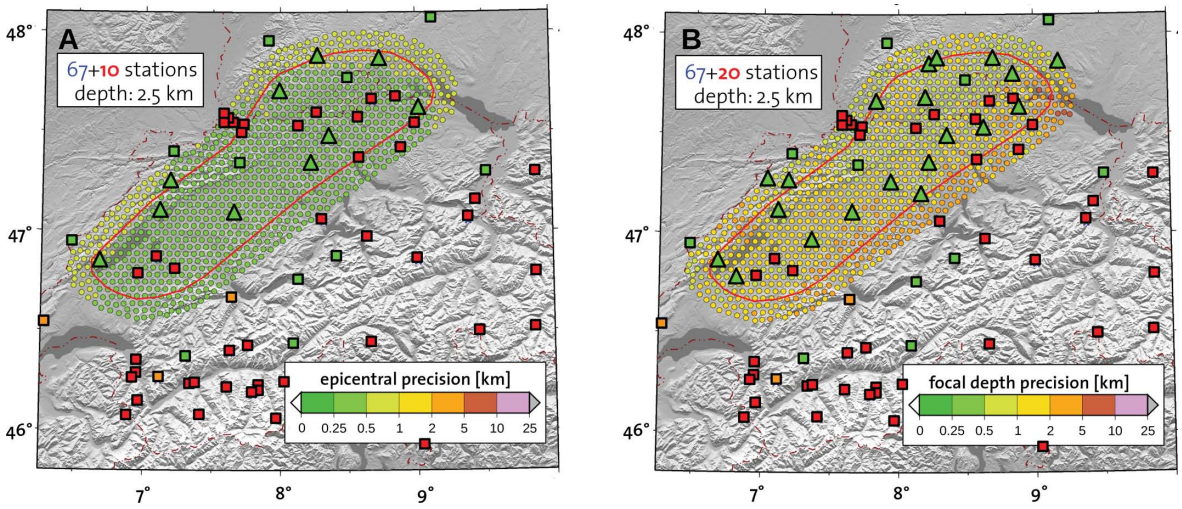

Figure 12. Optimization results for networks with 10 and 20 new stations (triangles) and 67 existing stations (squares). Colouring of the squares is identical to Fig. 10(B) and indicates observation rate. The colour of the virtual stations (dots) indicates location precision in 2.5 km depth for epicentral coordinates (A) and focal depth (B) derived with NonLinLoc.

resolution (Tarantola & Valette 1982). The solution is fully nonlinear, and, therefore, the resulting PDF may be irregular and multimodal. Uncertainty estimates derived from the posterior PDF are, in general, more reliable compared to those based on linearized methods (Lomax *et al.* 2000; Husen *et al.* 2013). In our approach we did not consider errors in the velocity model. Hence, absolute errors can be significantly larger than formal errors, presented here, especially in focal depth (e.g. Pavlis 1986).

As illustrated in Fig. 11, the error in epicentre and focal depth decrease constantly with increasing number of stations. The goal of reaching an overall error in epicentre of $2\sigma_h \leq 0.5$ km can already be achieved with a network of only 10 additional stations (Fig. 11A). Fig. 12(A) illustrates this result for the *D*-optimal network of this case by showing the 2σ epicentral errors for earthquakes located at a depth of 2.5 km. At this depth, $2\sigma_h$ shows a very homogenous distribution and is smaller than 0.5 km for most of the area of the earthquake perimeter. Only two small regions in the northeast and the southwest, outside of the earthquake perimeter have uncertainties up to 1 km. This observation can be explained by the poor network geometry (unfavourable azimuthal station distribution) in these regions.

Errors in focal depth are generally larger than those for epicentral coordinates (Fig. 11). This is a well-known fact that results from the geometry of the earthquake location problem with stations near the Earth's surface and earthquakes at depth (e.g. Gomberg *et al.* 1990). The predefined goal to obtain an overall focal-depth uncertainty of $2\sigma_z \leq 2.0$ km is reached for networks with 20 or more stations (Fig. 11B). The *D*-optimal network for this case is shown in Fig. 12(B). In general, the distribution of the focal-depth uncertainties is more heterogeneous than for the corresponding epicentral uncertainties. The focal-depth errors show a strong dependence on event-to-station distance, demonstrating the importance of stations at small epicentral distances to constrain focal depth (Fig. 12).

3.3 Estimation of expected magnitude of completeness, M_c

The expected magnitude of completeness, M_c, was estimated using the Bayesian Magnitude of Completeness (BMC) method introduced by Mignan *et al.* (2011). In a first step, we determined the spatial distribution of M_c observed in Switzerland in 20 km × 20 km spatial bins using earthquakes of the period between 2002 and 2008 from the ECOS2009 catalogue (Fäh *et al.* 2011). Then, we defined the network of observing stations by only selecting those stations that had at least 150 observations in the considered period. This value assured that only stations contributing to the location of at least 0.1 per cent of the events in our catalogue were used for the M_c estimation. Fig. 13(B) shows the 37 stations that met the selection criterion. All, except one Austrian station, belonged to the Swiss Seismological Network; 11 of the stations are inside of, or very close to, the earthquake perimeter and concentrate in the Basel area.

Using these inputs, we derived a functional relationship between M_c and the distance to the fourth observing station, d_4, following Mignan *et al.* (2011) and obtained the following result (see Fig. 13A):

$$M_c = 5.96 \cdot d_4^{0.08} - 6.44\,(\pm 0.16). \quad (9)$$

Using eq. (9), we were finally able to predict M_c at every location within Switzerland for arbitrary network geometries.

As indicated in Fig. 13(A), the scatter in the observed M_c-to-d_4 relationship is quite large. This may partly be due to the simplicity of the approach taken to define the observing network, where we only used a threshold for the minimum number of detections. Yet, comparing our M_c predictions for the existing network (Fig. 13B) with recent predictions of Nanjo *et al.* (2010, their fig. 3c), who dealt with network selection in a much more comprehensive way, we found a remarkably good agreement. The predicted values of M_c range between $M_c = 1.1$ and $M_c = 2.5$ for the region of Switzerland in both studies. Additionally, predictions for $M_c < 1.6$ were made for very similar areas in the Valais (SW Switzerland) and the Canton Aargau (NE Switzerland). In contrast to our prediction, Nanjo *et al.* (2010) found an additional region with $M_c < 1.6$ in Canton Graubünden (West Switzerland). Yet, they gave large uncertainties for that prediction (comp. their fig. 3d). The predictions made for the area of the earthquake perimeter are also highly similar in both studies with low values in the range of $M_c < 1.6$ in the northeast and larger values of $1.6 < M_c < 2.0$ in the central and southwestern part. The good agreement of the predictions of the two methods encouraged us to proceed with our simple and straightforward approach,

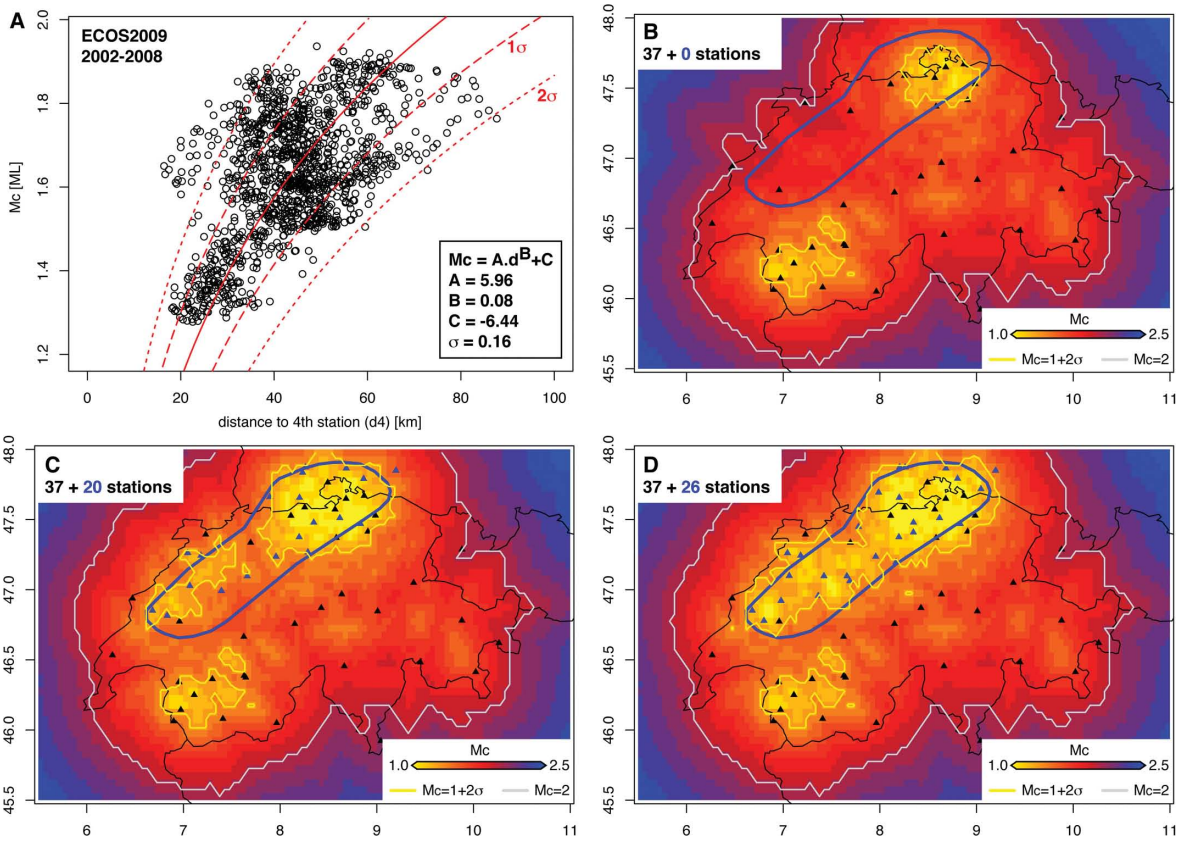

Figure 13. (A) Relationship between M_c and the distance to the fourth observing station d_4, derived for earthquakes between 2003 and 2008 in Switzerland from the ECOS2009 catalogue. The best fitting function in a least-squares sense, $M_c(d_4)$, is indicated in red with error intervals of 1σ and 2σ. (B–D) Predicted magnitude of completeness M_c for Switzerland and surrounding regions using the BMC method of Mignan *et al.* (2011). Predictions for the existing network (B), and networks with 20 (C) and 26 (D) new stations are shown. $M_c = 1$ is indicated by the light yellow colour, and contour lines correspond to the M_c levels indicated in the insets. 37 existing stations used for the M_c analysis are plotted as black triangles. New stations are shown as blue triangles. The earthquake perimeter is indicated by a blue polygon.

shown to be robust by Mignan *et al.* (2011) [see also Mignan (2012) regarding M_c estimation and Mignan *et al.* (2013) for an application of the BMC method to mainland China].

As shown, a network of 20 or more new stations is required to reach the anticipated hypocentral resolution in the study area. In the following, we will, therefore, discuss our M_c predictions at the example of networks with 20 and 26 new stations (Figs 13C and D). In both cases an improvement of the magnitude of completeness to $M_c < 1.6$ was predicted for the earthquake perimeter. However, it was also found that the anticipated value of $M_c = 1.0$ would only be reached in small parts of the study area. Yet, the BMC prediction has to be considered a conservative estimate of M_c, in that the detection capabilities of all stations are treated as equal and correspond to that of an average Swiss station. Additionally, considering the uncertainty in eq. (9) [$\sigma(M_c) = 0.16$], we feel that the upper error bound, indicated in Figs 13(C) and (D), may be a better estimate of the expected M_c in our case. If correct, this indicates that a network with 26 new stations could reach the desired magnitude of completeness over large parts of the study area.

4 DISCUSSION

4.1 Stability of the solution

It is apparent from eq. (7) that in simulated annealing the final solution depends on the generation of random numbers. In general, random numbers on computers are completely deterministic, in that they generate the exact same list of random numbers when initialized with the same start value, that is, the seed of the random number generator (Press *et al.* 1992). To test the stability of our solutions, we, therefore, ran 100 optimizations for the same network size with different seeds of the random number generator (reinitialized optimizations). In the following, the results will be discussed for a network with 20 new stations (Fig. 14), but they are equally valid for other network sizes.

The final values of the cost functions achieved in the 100 optimization runs showed only small variations, indicating very similar performance of the networks in all solutions. Only a small number of different network geometries was found, and the solution with the lowest cost function was chosen most often. Furthermore, the nCDFs for the errors in epicentre and focal depth were found to be nearly identical in every run, which indicates that the overall performance of the different networks was almost equal in all cases.

Networks with minimal, intermediate and maximal values of the cost function, representing the highest, intermediate and lowest overall location performance in the 100 optimization runs, are shown in Fig. 14. As can be inferred from the figure, the majority of new stations were placed at identical or very similar locations in different optimization runs. Even though network geometries for individual solutions differed in detail, we were able to identify stable regions of about 10 km diameter. Into these regions stations were

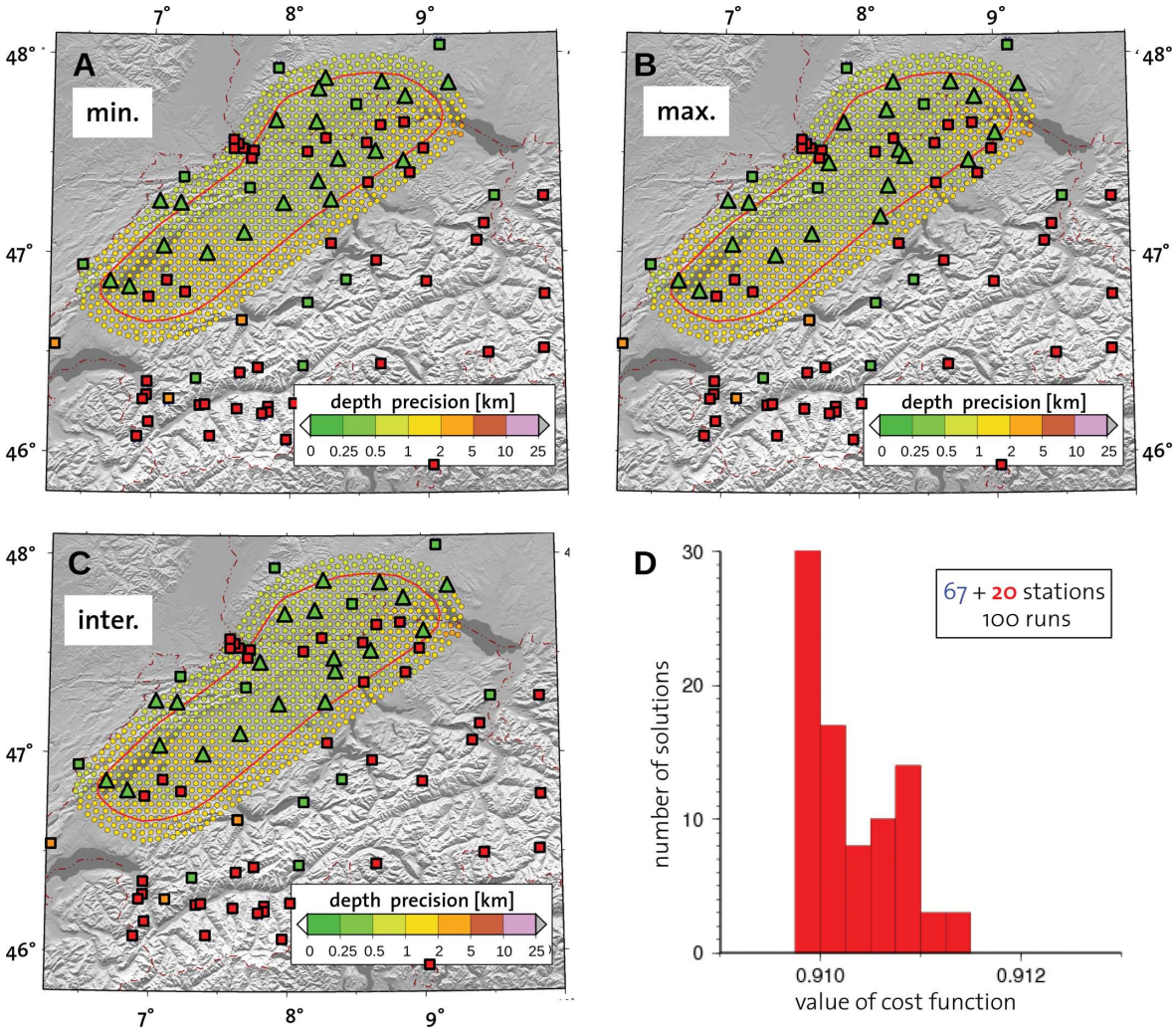

Figure 14. Stability of the optimization result to changes in the initialization of the random number generator. (A–C) Network geometries of the solutions with the minimal, intermediate and maximal achieved costs (Eq. 4). Symbols and colouring are identical to Fig. 12(B). (D) Histogram of the costs achieved in 100 optimization runs.

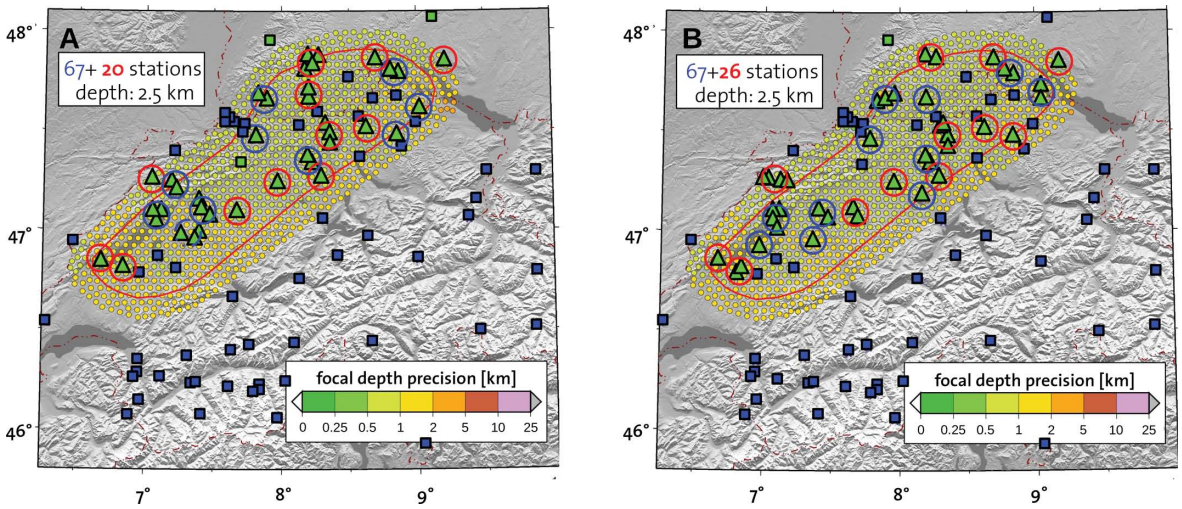

Figure 15. Definition of station placement regions for networks with 20 (A) and 26 (B) new stations. All station locations of the 10 best solutions (lowest cost function values) found in 100 reinitialized optimization runs (Fig. 14) are plotted. New stations are plotted as green triangles, existing stations as blue squares. Red and blue circles indicate placement regions with a diameter of 10 km. Red circles represent placement regions that contained stations in all considered solutions, and blue circles indicate regions that were empty at least once.

placed repeatedly in different optimization runs (Fig. 15). Many of these regions were selected, that is, contained a station, in all optimization runs and are marked by red circles in Fig. 15. The remaining regions were not selected in at least one of the optimization runs (blue circles in Fig. 15). Stations were only rarely placed at locations that were distant from locations found in other optimizations.

We interpret the variability of the solution as being due to the highly non-linear nature of the optimization problem. The solution space for these large-scale problems seems to contain many closely spaced minima that correspond to highly similar network geometries with similar uncertainty estimates in epicentre and focal depth. We accounted for this variability by defining site survey regions of approximately 10 km radius. This approach will also allow for the flexibility needed to find sites with the desired noise conditions in the field.

4.2 Network geometries

Not surprisingly, the noise class assigned to each station had a remarkably strong influence on the optimization results. Only virtual stations with noise class Low were selected in all performed optimizations. This can clearly be explained by the high observation rates found for stations with low noise levels (Fig. 10), which result in higher weights in the calculation of the cost function compared to stations with high and intermediate noise levels.

This argument also explains the observation that new stations were sometimes placed very close to existing stations associated with noise classes Middle or High (Figs 12B and 15). If an existing station at an important location has a small number of observations due to its high noise level, the optimization algorithm tries to put more weight on this location by placing a new station at a nearby location associated with noise class Low.

A similar explanation can be given for the observation that new stations clustered at neighbouring positions, especially for increasing network size (Figs 12B and 15). If a study area is already monitored by a sufficiently large network with a nearly optimal configuration, the value of the cost function can most efficiently be further reduced by adding a station at the, already occupied, most important location. In this way the weight of the most important station is doubled when computing the cost function. For a large nearly optimal network this strategy will, in general, cause a larger decrease of the cost value than optimization without allowed co-location. This is because, in the latter case many stations of the network have to be relocated to less optimal positions to accept an additional station. In our algorithm we did not allow for exact co-location, this is why the optimization placed stations on gridpoints neighbouring the most important station, to reproduce the strategy outlined above as close as possible.

In general, the clustering of stations at nearby locations is a consequence of our algorithm ignoring the correlation of model errors (e.g. Rabinowitz & Steinberg 1990). This effect could have been accounted for by introducing a station-distance weight when calculating the cost function (e.g. Hardt & Scherbaum 1994). We decided not to do so. Motivated by the explanation given earlier, we interpret the clustering of stations at a site as an indication for the importance of that location. Even more so, if the placement regions were stable in solutions for different network sizes. The last observation indicates that station locations exist that are important for the hypocentral resolution of a region independent of the planned network size.

4.3 Network size

It has to be concluded from the results presented that it is an ambitious goal to reach a constant completeness of $M_c = 1$ over a large area of several hundred square kilometres. This aim can only be realizable if an unrealistically high number of new stations would be installed. For example, we can derive the distance to the fourth station that a network must provide to assure a completeness of $M_c = 1.0$ from eq. (9), and obtain a value of $d_4 = 16 \pm 5$km for Switzerland. Let us assume for simplicity that we want to cover a rectangular study area with dimensions of $a \times b\,\mathrm{km}^2$ by a regular square-gridded network. With a grid spacing $s = d_4/\sqrt{2}$ we can assure that the maximum event–station distance inside this network is equal to d_4, and thus the completeness $M_c = 1$. The number of stations, N_s, needed for this network can be calculated by

$$N_s = (\mathrm{ceil}\,(a/s) + 1) \times (\mathrm{ceil}\,(b/s) + 1), \tag{10}$$

where function ceil(A) rounds A to the nearest integer greater than or equal to A. Inserting the appropriate values for our study area in eq. (10), we estimate a need of 114 stations in total to meet the M_c requirement. This estimate is valid for stations with a noise level corresponding to a weighted mean of the station noise levels used in the BMC estimation. Assuming that the lower and upper uncertainty limits in eq. (9) represent values for high- and low-noise stations, we need to adapt our need estimate to 75 low-noise stations or 175 high-noise stations, respectively.

We have to point out that the network geometry in the example mentioned above was chosen for illustrative purposes only, and is neither optimal with respect to the number of stations needed to meet the M_c requirement, nor to earthquake location. We are working on the implementation of the M_c requirement into the optimization process.

What the exact meaning of low, mean or high noise level is in the context of BMC is hard to quantify, and needs to be addressed in a separate study. We think that the level of $v_{rms} = 60\,\mathrm{nm\,s}^{-1}$, used for noise class Middle in the optimization, represents a conservative upper limit to the mean noise level governing the BMC calculation. This is because, stations of good quality are most probably used preferentially for earthquake location, and, therefore, also dominate the derivation of the d_4–M_c relationship.

Yet, a general conclusion can be drawn from the strong dependence of the station need on d_4, and thus on the noise levels of the stations. A careful assessment of the noise levels of potential station locations assuring the selection of high-quality sites in a placement region is essential for the successful obtainment of the M_c requirements imposed on a new network. A quantitative strategy for the evaluation and selection of high-quality station locations was recently introduced by Plenkers *et al.* (2012).

On the other hand, the probability of recording M_L 1 earthquakes in a region where $M_c < 1.6$ is still rather high (compare Nanjo *et al.* 2010). Depending on the scientific targets of the planned network, it may, therefore, be acceptable to relax the M_c constraint for parts of a study area.

5 CONCLUSIONS

We have developed a network optimization approach based on the *D*-criterion and extended the algorithm of Hardt & Scherbaum (1994) to handle 3-D velocity models, correctly deal with existing stations and the case of non-detections at specific sites. The

algorithm was successfully tested with simple well-studied test cases.

A first-order ambient noise model for Switzerland was developed on the basis of land-use data from satellite imagery. The model agrees well with observed noise levels at 67 existing stations in Switzerland, Austria and Germany. In combination with calculated *P*-wave amplitudes of synthetic earthquakes, the noise model was used to identify non-detections at the virtual stations. The optimization was found to be strongly dependent on the ambient noise model, as only virtual stations with the lowest noise class were used in *D*-optimal solutions. It has to be concluded that it is very important to update the ambient noise model by ground motion measurements and to reevaluate the optimization result as soon as possible in the network implementation process.

We have applied the algorithm to a large-scale network optimization problem for a regional-scale microseismic network in NE Switzerland. We were able to find the size and geometry of *D*-optimal networks that fulfil the predefined criteria concerning hypocentral resolution. A minimum number of 20 new stations is needed to achieve a hypocentral resolution of 2 km in the study area. An epicentral resolution of 0.5 km can already be reached with a network of 10 new stations. The hypocentral uncertainty predictions were confirmed by computing fully probabilistic non-linear uncertainty estimates.

The sensitivity of the networks to detect small earthquakes was assessed by estimating the expected magnitude of completeness in the region of interest. The results indicate that it is an ambitious goal trying to reach a constant magnitude of completeness of $M_c = 1.0$ over a large area of several hundred square kilometres. For the microseismic network in NE Switzerland we conclude that this goal will not be reached with a network of 20 new stations and only partly with a network of 26 new stations. On the other hand, the probability of recording M_L 1 earthquakes in a region where $M_c < 1.6$ is still rather high (compare Nanjo *et al.* 2010). Depending on the scientific goals of the planned network it may, therefore, be acceptable to relax the M_c constraint for parts of a study area.

The stability of the solutions obtained for the regional-scale network was tested by repeated optimizations with reinitializing the random number generator (reinitialized solutions). The overall hypocentral resolutions for all reinitialized solutions of a certain network size were found to be nearly identical, even though the network geometries showed small variations. Yet, it was possible to identify placement regions with a diameter of approximately 10 km that were stable for solutions of the same network size and, to some extent, also for different network sizes.

In general, we conclude that a stepwise approach should be taken to identify the number and location of new stations for regional-scale networks. First, stable placement regions should be identified by finding *D*-optimal geometries for networks of different sizes and by repeated reinitialized optimization. Important placement regions can be identified as being those most frequently selected during this procedure and should be instrumented with high priority. Once instrumented, the recorded noise levels from these regions can be used to update the network optimization and to define the locations of the remaining stations. This procedure should be repeated until the desired hypocentral resolution and sensitivity of the network are reached.

In the way indicated earlier, we defined 10 site survey regions for the first instrumentation phase of the network in NE Switzerland. These regions existed in solutions for networks of 20 and 26 new stations, and were stable in the reinitialized optimizations (Fig. 15). If such a region contained an existing station with a high noise level, we considered relocating the station to an alternative site with a lower noise level, or to relocate the seismometer into a shallow borehole.

In this study, we have not considered the problem of temporal station failure that can reduce the capability of a network to detect and locate earthquakes. However, the future network, under discussion in the study, will consist of permanent stations with reliable real-time data transmission, that is, permanent dedicated telephone lines. Therefore, data quality and availability can and will be monitored continuously, and problems can be detected and solved quickly by the duty technician. From our analysis of SED stations of this type, we expect a mean data availability of about 99 per cent, which corresponds to 361 of 365 days (Kraft 2012). As the main goal of the network will be to improve the understanding of the neotectonic activity of the study area, we consider downtime of less than 1 per cent as acceptable. Nevertheless, it is essential to say that for sparse networks, when expecting significantly higher station downtimes, or in an earthquake alarming or early-warning context, redundant instrumentation of important placement regions has to be considered.

ACKNOWLEDGEMENTS

We thank the National Cooperative for the Disposal of Radioactive Waste (NAGRA) and the Project GEOBEST funded by the Swiss Federal Office of Energy for the support of this study. We are deeply indebted to Frank Scherbaum for providing the C source code originally developed in Matthias Hardt's diploma thesis in 1992. Matteo Spada (SED) and Falko Bethmann (now GeoEnergy Suisse AG) are acknowledged for compiling the synthetic earthquake catalogues and calculating non-linear probabilistic earthquake locations using NonLinLoc, respectively. We are grateful for many discussions with Michael Schnellman (NAGRA), Stephan Husen, Katrin Plenkers, Jochen Wössner and Florian Haslinger (SED). We like to thank our colleagues of the FKPE working group Induced Seismicity Joachim Ritter, Jörn Groos, Thomas Plenefisch, Joachim Wassermann, Stefan Baisch and Ralf Fritschen for useful discussions on noise level classification.

Eventually, we thank three anonymous reviewers and the editor for their comments, which helped to improve the manuscript significantly.

REFERENCES

Aki, K. & Richards, P.G., 1980. *Quantitative Seismology, Theory and Methods*, Vol. 1, Freeman and Company, San Francisco, 1–557.

Bartal, Y., Somer, Z., Leonard, G., Steinberg, D.M. & Ben Horin, Y., 2000. Optimal seismic networks in Israel in the context of the Comprehensive Test-Ban Treaty, *Bull. seism. Soc. Am.*, **90**(1), 151–165.

Basu, A. & Frazer, L.N., 1990. Rapid determination of the critical temperature in simulated annealing inversion, *Science*, **249,** 1409–1412.

Bay, F., Fäh, D., Malagnini, L. & Giardini, D., 2003. Spectral shear wave ground motion scaling in Switzerland, *Bull. seism. Soc. Am.*, **93**(1), 414–429.

Bay, F., Wiemer, S., Fäh, D. & Giardini, D., 2005. Predictive ground motion scaling in Switzerland: best estimates and uncertainties, *J. Seismol.*, **9**(2), 223–240.

Benz, H.M., Chouet, B.A., Dawson, P.B., Lahr, J.C., Page, R.A. & Hole, J.A., 1996. Three-dimensional P and S wave velocity structure of Redoubt Volcano, Alaska, *J. geophys. Res.*, **101**(B4), 8111–8128.

Bohnhoff, M., Dresen, G., Ellsworth, W.L. & Ito, H., 2010. Passive seismic monitoring of natural and induced earthquakes: case studies, future directions and socio-economic relevance, in *New Frontiers in Integrated Solid Earth Sciences*, pp. 261–285, eds Cloetingh, S. & Negendank, J., Springer, Heidelberg.

Bormann, P., 1998. Conversion and comparability of data presentations on seismic background noise, *J. Seismol.*, **2,** 37–45.

Brune, J.B., 1970. Tectonic stress and spectra of seismic shear waves from earthquakes, *J. geophys. Res.*, **75**(26), 4997–5009.

Brune, J.B., 1971. Correction, *J. geophys. Res.*, **76**(20), 5002.

Buland, R., 1976. The mechanics of locating earthquakes, *Bull. seism. Soc. Am.*, **66**(1), 173–187.

Büttner, G., Feranec, J., Jaffrain, G., Man, L., Maucha, G. & Soukup, T., 2004. The CORINE Land Cover 2000 Project, *EARSeL eProc.*, **3**(3), 331–346.

Edwards, B., Allmann, B., Fäh, D. & Clinton, J., 2010. Automatic computation of moment magnitudes for small earthquakes and the scaling of local to moment magnitude, *Geophys. J. Int.*, **183**(1), 407–420.

England, P. & Jackson, J., 2011. Uncharted seismic risk, *Nature Geosci.*, **4,** 348–349.

Fäh, D. *et al.*, 2003. Earthquakes catalogue of Switzerland (ECOS) and the related macroseismic database, *Eclogae Geol. Helv.*, **96,** 219–236.

Fäh, D. *et al.*, 2011. *ECOS-09 earthquake catalogue of Switzerland release 2011 report and database. Public catalogue, 17. 4. 2011. Swiss Seismological Service ETH Zurich*, Report SED/RISK/R/001/20110417. Available at: http://www.seismo.ethz.ch/static/ecos-09/ECOS-2009_Report_final_WEB.pdf, Last accessed 13 June 2013.

Farr, T.G. *et al.*, 2007. The shuttle radar topography mission, *Rev. Geophys.*, **45**(RG2004), doi:10.1029/2005RG000183.

Flinn, E.A., 1965. Confidence region and error determinations for seismic event location, *Rev. Geophys.*, **3**(1), 157–185.

Giardini, D., Wiemer, S., Fäh, D. & Deichmann, N., 2004. *Seismic hazard assessment of Switzerland. Swiss Seismological Service at ETH Zurich*. Available at: http://www.seismo.ethz.ch/prod/haz_map/hazard_report, Last accessed 13 June 2013.

Goertz, A., Riahi, N., Kraft, T. & Lambert, M., 2012. Modeling detection thresholds of microseismic monitoring networks, *SEG Technical Program Expanded Abstracts*, 1–6. [http://dx.doi.org/10.1190/segam2012-1069.1]

Gomberg, J.S., Shedlock, K.M. & Roecker, S.W., 1990. The effect of S-wave arrival times on the accuracy of hypocenter estimation, *Bull. seism. Soc. Am.*, **80**(6), 1605–1628.

Grassberger, P. & Procaccia, I., 1983. Measuring the strangeness of strange attactors, *Physica*, **9D,** 189–208.

Gutenberg, B. & Richter, C.F., 1944. Frequency of earthquakes in California, *Bull. seism. Soc. Am.*, **34,** 185–188.

Hardt, M. & Scherbaum, F., 1994. The design of optimum networks for aftershock recordings, *Geophys. J. Int.*, **117**(3), 716–726.

Husen, S., Kissling, E., Deichmann, N., Wiemer, S., Giardini, D. & Baer, M., 2003. Probabilistic earthquake location in complex three-dimensional velocity models: application to Switzerland, *J. geophys. Res.*, **108**(B2), doi:10.1029/2002JB001778.

International Atomic Energy Agency, 2002. *Evaluation of Seismic Hazards for Nuclear Power Plants, IAEA Safety Standards Series, Safety Guide No. NS-G-3.3*, IAEA, Vienna, 31 pp.

Kastrup, U., Zoback, M.L., Deichmann, N., Evans, K.F., Giardini, D. & Michael, A.J., 2004. Stress field variations in the Swiss Alps and the northern Alpine foreland derived from inversion of fault plane solutions, *J. geophys. Res.*, **109,** B01402, doi:10.1029/2003JB002550.

Kijko, A., 1977. An algorithm for the optimum distribution of a regional seismic network—I, *Pageoph*, **115,** 999–1009.

Kirkpatrick, S., Gelatt, C.D. & Vecchi, M.P., 1983. Optimization by simulated annealing, *Science*, **220,** 671–680.

Kraft, T., 2012, Installationsbericht: Seismologisches Überwachungsnetz für das Geothermieprojekt der Stadt Sankt Gallen, unpublished report of the Swiss Seismological Service, 1–39.

Lee, W.H.K. & Stewart, S.W., 1981. Principles and applications of microearthquake networks, *Adv. Geophys.*, (Suppl. 2), 1–293.

Lilwall, R.C. & Francis, T.J.G., 1978. Hypocentral resolution of small ocean bottom seismic networks, *Geophys. J. R. astr. Soc.*, **54**(3), 721–728.

Lomax, A., Virieux, J., Volant, P. & Berge, C., 2000. Probabilistic earthquake location in 3D and layered models: introduction of a Metropolis-Gibbs method and comparison with linear locations, in *Advances in Seismic Event Location*, pp. 101–134, eds Thurber, C. & Rabinowitz, N., Kluwer, Amsterdam.

McNamara, D.E. & Boaz, R.I., 2005. Seismic noise analysis system using power spectral density probability density function: a stand-alone software package. Open-File Rep, U.S. Geol. Surv., **30,** 2005–1438.

Menke, W., 1989. *Geophysical Data Analysis: Discrete Inverse Theory*, Academic Press, New York, 1–289.

Metropolis, N., Rosenbluth, A.W., Rosenbluth, M., Teller, A.H. & Teller, E., 1953. Equation of state calculations by fast computing machines, *J. Chem. Phys.*, **21,** 1087–1092.

Mignan, A., 2012. Functional shape of the earthquake frequency-magnitude distribution and completeness magnitude, *J. geophys. Res.*, **117,** B08302, doi:10.1029/2012JB009347.

Mignan, A., Werner, M.J., Wiemer, S., Chen, C.C. & Wu, Y.M., 2011. Bayesian estimation of the spatially varying completeness magnitude of earthquake catalogs, *Bull. seism. Soc. Am.*, **101**(3), 1371–1385.

Mignan, A., Jiang, C., Zechar, J.D., Wiemer, S., Wu, Z. & Huang, Z., 2013. Completeness of the Mainland China earthquake catalog and implications for the setup of the China Earthquake Forecast Testing Center, *Bull. seism. Soc. Am.*, **103,** doi:10.1785/0120120052.

Minster, J.B., Jordan, T.H., Molnar, P. & Haines, E., 1974. Numerical modeling of instantaneous plate tectonics, *Geophys. J. R. astr. Soc.*, **36**(3), 541–576.

Müller, G., 1986. *Theorie elastischer Wellen, Lecture Notes*, Institute of Meteorology and Geophysics, University of Frankfurt, 120 pp.

Nanjo, K.Z., Schorlemmer, D., Woessner, J., Wiemer, S. & Giardini, D., 2010. Earthquake detection capability of the Swiss seismic network, *Geophys. J. Int.*, **181**(3), 1713–1724.

Pavlis, G.L., 1986. Appraising earthquake hypocenter location errors: a complete, practical approach for single-event locations, *Bull. seism. Soc. Am.*, **76**(6), 1699–1717.

Persson, P.-O. & Strang, G., 2004. A simple mesh generator in MATLAB, SIAM Review, *SIAM J. Applied Math*, **46**(2), 329–345.

Peters, D.C. & Crosson, R.S., 1972. Application of prediction analysis to hypocenter determination using local arrays, *Bull. seism. Soc. Am.*, **62**(3), 775–788.

Plenkers, K., Kraft, T., Bethmann, F., Husen, S. & Schnellmann, M., 2012. Optimizing site selection in urban areas in northern Switzerland, *EGU General Assembly Conference Abstracts*, **14,** 7107.

Podvin, P. & Lecomte, I., 1991. Finite difference computations of travel-times in very contrasted velocity models: a massively parallel approach and its associated tools, *Geophys. J. Int.*, **105,** 271–284.

Press, W., Flannery, B., Teukolsky, S. & Vetterling, W., 1992. *Numeric Recipes in C: The Art of Scientific Computing*, Cambridge University Press, New York, 1–994.

Rabinowitz, N. & Steinberg, D.M., 1990. Optimal configuration of a seismographic network: a statistical approach, *Bull. seism. Soc. Am.*, **80**(1), 187–196.

Satake, K., 1985. Effects of station coverage on moment tensor estimation, *Bull. seism. Soc. Am.*, **75**(6), 1657–1667.

Souriau, A. & Woodhouse, J.H., 1985. A strategy for deploying a seismological network for global studies of earth structure, *Bull. seism. Soc. Am.*, **75**(4), 1179–1193.

Steinberg, D.M. & Rabinowitz, N., 2003. Optimal seismic monitoring for event location with application to on site inspection of the comprehensive nuclear test ban treaty, *Metrika*, **58**(1), 31–57.

Swiss Federal Statistical Office, 2011. http://www.bfs.admin.ch/bfs/portal/en/index.htm, Last accessed 13 June 2013.

Tarantola, A. & Valette, B., 1982. Generalized nonlinear inverse problems solved using the least squares criterion, *Rev. geophys. Space Phys.*, **20**(2), 219–232.

Uhrhammer, R.A., 1980. Analysis of small seismographic station networks, *Bull. seism. Soc. Am.*, **70**(4), 1369–1379.

Wiemer, S. & Wyss, M., 2000. Minimum magnitude of completeness in earthquake catalogs: examples from Alaska, the western United States, and Japan, *Bull. seism. Soc. Am.*, **90**(4), 859–869.

Zayats, N. & Steinberg, D.M., 2010. Optimal design of experiments when factors affect detection capability, *Pak. J. Statist.*, **26**(1), 15–37.